ORGANOMETALLICS

Interplay of Charge and Aromaticity Upon Chemical Reduction of *p*-Quinquephenyl with Alkali Metals

Matthew Pennachio, Zheng Zhou, Zheng Wei, Alexandra Tsybizova, Renana Gershoni-Poranne,* and Marina A. Petrukhina*

Cite This: *Organometallics* 2023, 42, 2492−2504

Read Online

ACCESS | Metrics & More | Article Recommendations | Supporting Information

ABSTRACT: Chemical reduction study of a paraphenylene comprising five *para*-connected aromatic rings, namely, *p*-quinquephenyl ($C_{30}H_{22}$, **1**), with alkali metals in THF revealed a facile formation of the doubly reduced anion, **1²⁻**, which was crystallized with different alkali metal counterions. Several products were characterized using single-crystal X-ray diffraction and spectroscopic methods. The use of different alkali metals allowed tuning of metal binding in the resulting crystalline products. The consequences of electron addition and metal complexation on the core of *p*-quinquephenyl were investigated with the help of computational methods. Most notably, reduction results in a shift from locally aromatic to quinoidal character of **1²⁻**, which is mitigated by complexation to the alkali metal cations.
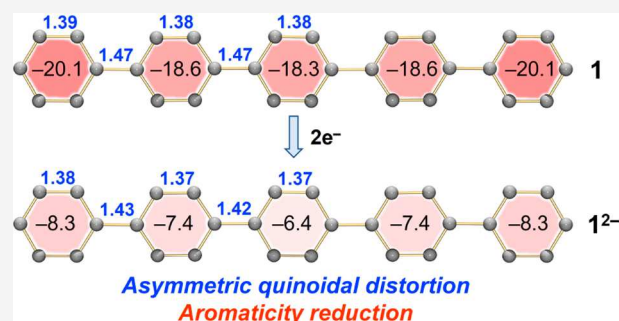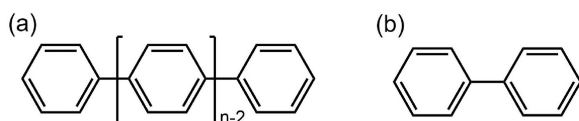

■ INTRODUCTION

The reduction of polycyclic aromatic hydrocarbons (PAHs) has attracted significant attention over recent years, inspired by fundamental chemistry and material science applications.[1−5] Chemical reduction of PAHs with alkali metals enables the formation of charged π-conjugated carbanions with positive and negative curvatures, which undergo structural deformation,[6−18] core transformation,[19−23] and reductive dimerization processes.[24−27] Moreover, the alkali metal intercalated products of PAHs have shown interesting quantum phenomena,[28] thus stimulating the developments of new molecular materials with intriguing electronic,[29−31] conducting,[32−38] and magnetic properties.[39,40]

Among a wide variety of PAHs, linear paraphenylenes, chain-like organic compounds comprising a certain number of *para*-connected aromatic rings (Scheme 1a),[41,42] have been realized as promising materials in molecular electronics and nanotechnology due to their conductivity, high thermal and oxidative stability, and compressive mechanical property. The shortest paraphenylene, biphenyl (Scheme 1b), occurring naturally in petroleum, has been widely studied as a charge/energy transfer salt in preparation of nanocarbons,[43] as well as

an electrolyte additive for lithium-ion batteries.[44] Over the course of several decades, despite many reports on poly-*p*-phenylenes, the synthesis of longer paraphenylenes with certain lengths has remained challenging due to their poor solubility. To date, the longest paraphenylene successfully synthesized is *p*-nonaphenylene ($n = 9$),[45] but the longest one for which structural characterization was accomplished is *p*-septiphenyl ($n = 7$).[46]

Unlike [*n*]cycloparaphenylenes ([*n*]CPPs,[47] the segments of armchair carbon nanotubes), the HOMO−LUMO gaps of linear paraphenylenes narrow as the number of aromatic rings is increased,[48] and they can become p- or n-type semiconducting materials upon complexation. The study of conductivity of paraphenylenes was initiated by Baughman et al. in 1979[49] and was recently developed by Ren et al.[50,51] It was found that paraphenylenes can be converted from electrical insulators to highly conducting charge transfer complexes when doped with electron donors (Li, Na, or K) or electron acceptors (AsF_5, SbF_5, or BF_3). In addition, Chen et al. demonstrated the superconductivity of a series of potassium-doped paraphenylenes ($n = 2−5$), with T_c values measured up to 123 K.[52−55] However, an in-depth understanding of doping, charge transfer effects, and structure−

Scheme 1. Depictions of (a) Paraphenylenes and (b) Biphenyl

Scheme 2. Chemical Reduction of 1 with Group 1 Metals in THF

Li, THF, 24 h → [Li$^+$(THF)$_4$]$_2$[(1^{2-})]·0.4THF (2·0.4THF)

Na, THF, 8 h → [{Na$^+$(THF)$_3$}$_2$(1^{2-})] (3)

K, THF, 6 h / 18-crown-6 → [{K$^+$(18-crown-6)(THF)}$_2$(1^{2-})] (4)

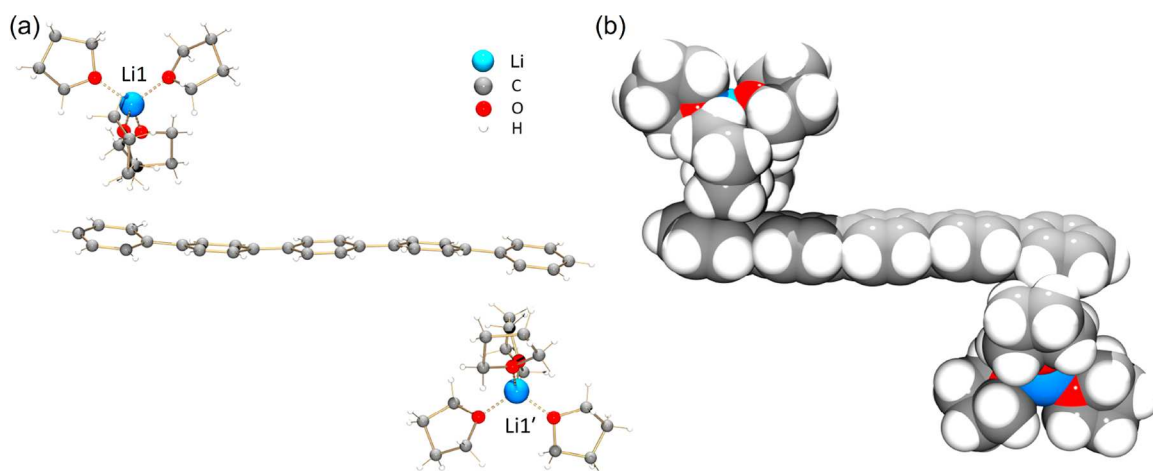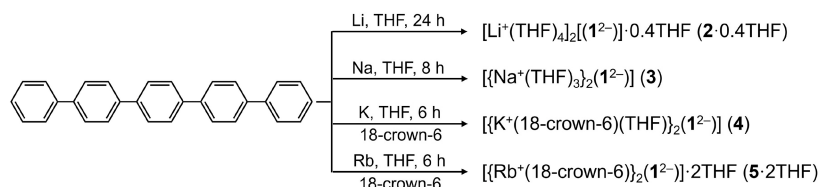Rb, THF, 6 h / 18-crown-6 → [{Rb$^+$(18-crown-6)}$_2$(1^{2-})]·2THF (5·2THF)

Figure 1. Crystal structure of **2**: (a) ball-and-stick and (b) space-filling models.

property correlations has been limited due to the lack of single-crystalline materials.

Charging PAHs with electrons and elucidating the structural and electronic consequences is not only of great significance in fundamental chemistry, but also enables better understanding of the corresponding materials properties. For shorter paraphenylenes, chemical reduction processes have been well studied through cyclic voltammetry,[56] spectroscopic techniques,[57−59] and computational methods.[60] A plethora of information exists in the scientific literature on the chemical reduction of the simplest paraphenylene, biphenyl,[61−63] which undergoes two-electron reduction accompanied by the formation of a dianionic quinoid structure. Moreover, p-terphenyl (n = 3) and p-quarterphenyl (n = 4) can readily accept up to two electrons, affording the doubly reduced products with sodium counterions, which can turn on/off their binding to the charged anionic core.[64,65]

In terms of longer paraphenylenes, such as p-quinquephenyl (n = 5) containing five phenyl rings linearly linked through the para-positions,[46] the electrochemical study of in situ generated radical anions and cations through Raman spectroscopy has been reported by Tasumi et al.[66] However, no chemical reduction or X-ray crystallographic data on the reduced products have been reported up to date. Herein, we carry out a broad investigation of the chemical reduction behavior of p-quinquephenyl (1) with Group 1 metals ranging from lithium to rubidium. As a result, a family of the doubly reduced p-quinquephenyl anions has been prepared with the corresponding alkali metal counterions and fully characterized using single-crystal X-ray diffraction and NMR and UV−vis spectroscopy. A computational analysis has been performed to elucidate the electronic structures of the studied compounds.

■ RESULTS AND DISCUSSION

Chemical Reduction of p-Quinquephenyl and Crystallographic Study of its Doubly-Reduced Products. The chemical reduction of **1** with Group 1 metals has been investigated in THF at room temperature. Using UV−vis absorption spectroscopy, a quick color change from purple (530 nm) to blue (321 nm) has been detected in all cases (Figures S1−S4). This is indicative of a two-step reduction process and the intermediate monoreduced state of **1** can be detected by EPR spectroscopy (Figure S21). By slow diffusion of hexanes into the THF reaction solutions (Scheme 2), dark purple needles or blocks have been isolated in moderate yield within 7 days. Single-crystal X-ray diffraction analysis confirmed the formation of a solvent-separated ion product of the doubly reduced anion, **1**$^{2-}$, with Li$^+$ counterions, [Li$^+$(THF)$_4$]$_2$[(1^{2-})] (crystallized with 0.4 interstitial THF molecule as **2·0.4THF**), and a complex with Na$^+$ counterions, [{Na$^+$(THF)$_3$}$_2$(1^{2-})] (**3**). Additionally, when 18-crown-6 ether was added during crystallization, two complexes of **1**$^{2-}$ with K$^+$ and Rb$^+$ counterions were isolated, namely, [{K$^+$(18-crown-6)(THF)}$_2$(1^{2-})] (**4**) and [{Rb$^+$(18-crown-6)}$_2$(1^{2-})] (crystallized with 2 interstitial THF molecules as **5·2THF**).

In the crystal structure of **2**, there are five crystallographically independent Li$^+$ ions and two and a half independent **1**$^{2-}$ anions (Figure S21), thus the values discussed below are averaged. The Li$^+$ ions are solvent-separated from the "naked" **1**$^{2-}$ dianion (Figure 1), allowing investigation of the paraphenylene core upon 2-fold reduction without direct metal binding influence. The coordination of each Li$^+$ cation is completed by four THF molecules, with the Li−O$_{THF}$ distances ranging from 1.862(10) Å to 1.929(9) Å, which are close to those previously reported.[10,22,67]

The crystal structure of **3** contains two crystallographically independent Na$^+$ ions (Figure S23). The Na1 ion is bound to the central phenyl ring of **1**$^{2-}$ in an asymmetric η^2-fashion, with
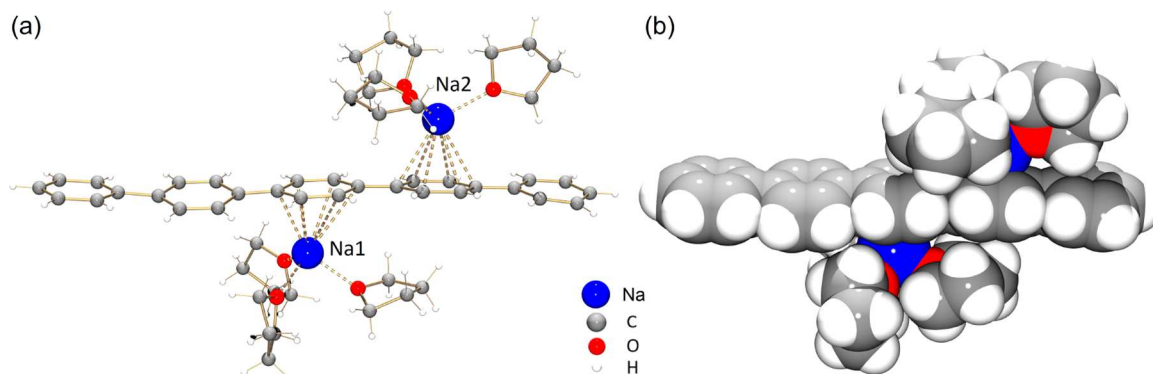
Figure 2. Crystal structure of **3**: (a) ball-and-stick and (b) space-filling models.
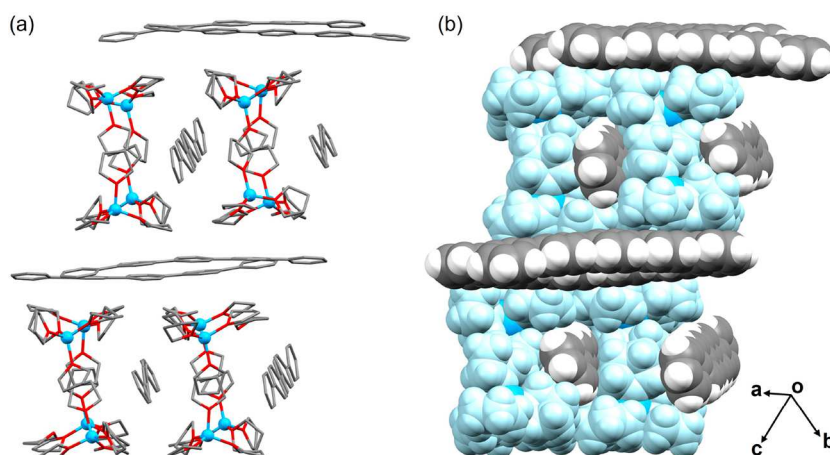

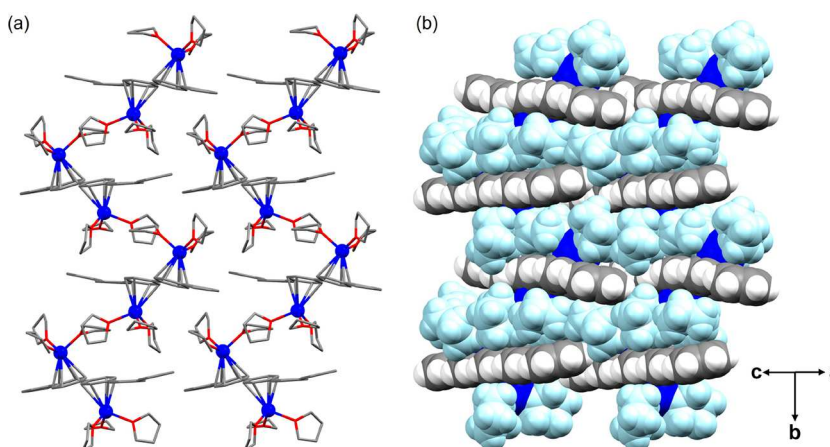**Figure 3.** Solid-state packing in **2**: (a) mixed (no H atoms) and (b) space-filling models.

Figure 4. Solid-state packing in **3**: (a) mixed (no H atoms) and (b) space-filling models.

the Na–C distances ranging over 2.649(7)−3.131(8) Å (Figure 2). Notably, the Na2 ion is η^6-coordinated to the adjacent phenyl ring with a smaller range of Na–C distances (2.86(4)−2.93(4) Å). This asymmetric metal binding of Na$^+$ ions has been observed in a shorter paraphenylene *p*-terphenyl, with the Na$^+$ ions being coordinated to either two different phenyl rings or the same one.[64,65] Both Na$^+$ ions are capped by three THF molecules, and the Na–O$_{THF}$ distances of 2.19(4)−2.301(8) Å are consistent with those previously reported.[68−71]

In the solid-state structure of **2** (Figure 3), multiple C−H···π contacts are found between the **1**$^{2-}$ anions and the {Li$^+$(THF)$_4$} cations, with the distances spanning over 2.499(13)−2.803(13) Å. The relatively loose packing of this crystal structure results in the formation of a 3D network, where the **1**$^{2-}$ anions are packed in two directions. In the solid-state structure of **3**, a 3D network is formed through C−H···π interactions (2.755(10)−2.813(10) Å) between the **1**$^{2-}$ anions and the coordinated THF molecules of the cations. In contrast to **2**, the **1**$^{2-}$ anions in **3** are nearly aligned in the same direction (Figure 4).
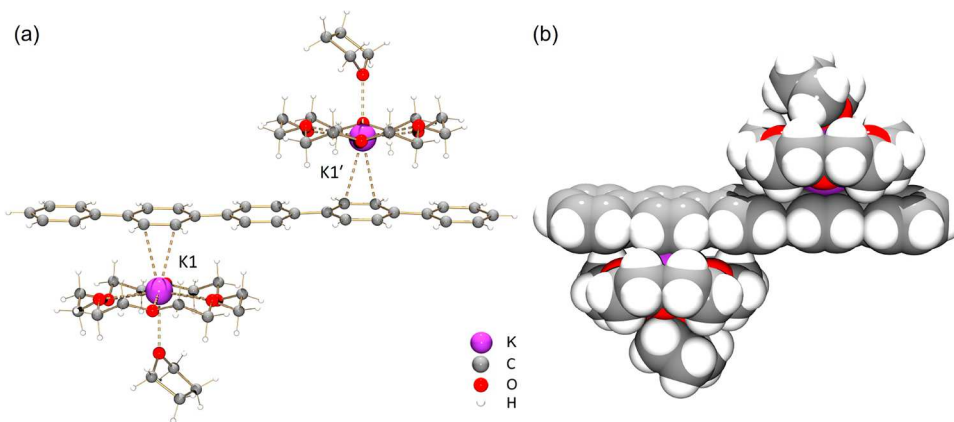
Figure 5. Crystal structure of **4**: (a) ball-and-stick and (b) space-filling models.
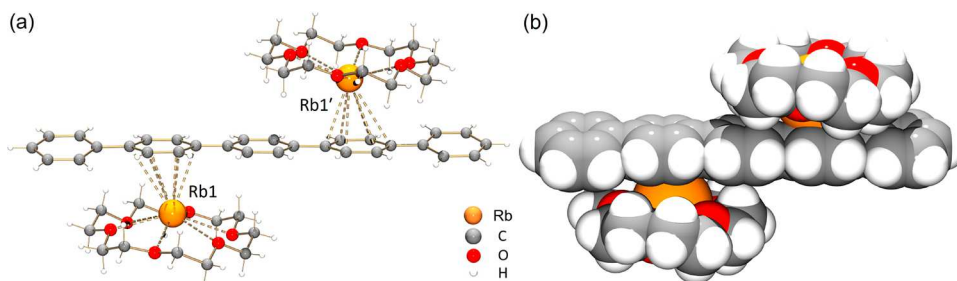
Figure 6. Crystal structure of **5**: (a) ball-and-stick and (b) space-filling models.
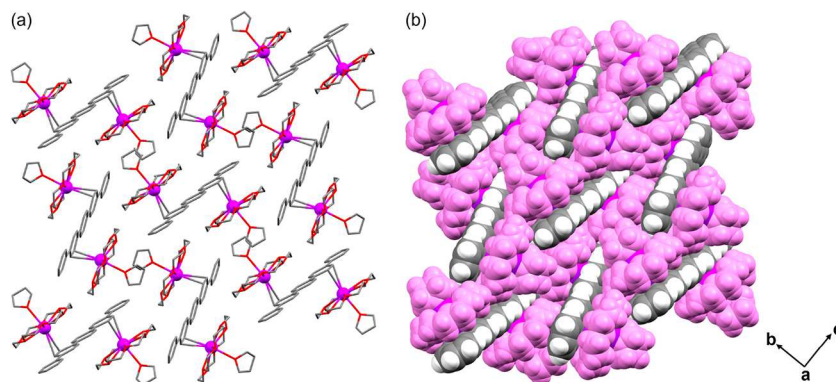
Figure 7. Solid-state packing in **4**: (a) mixed (no H atoms) and (b) space-filling models.

Figure 8. Solid-state packing in **5**: (a) mixed (no H atoms) and (b) space-filling models.

In the crystal structure of **4**, there is only one crystallographically independent K$^+$ ion (Figure S25). The K$^+$ ion is η^2-

coordinated to the phenyl ring next to the central one, with the K−C distances of 3.168(3) Å and 3.189(3) Å (Figure 5). A

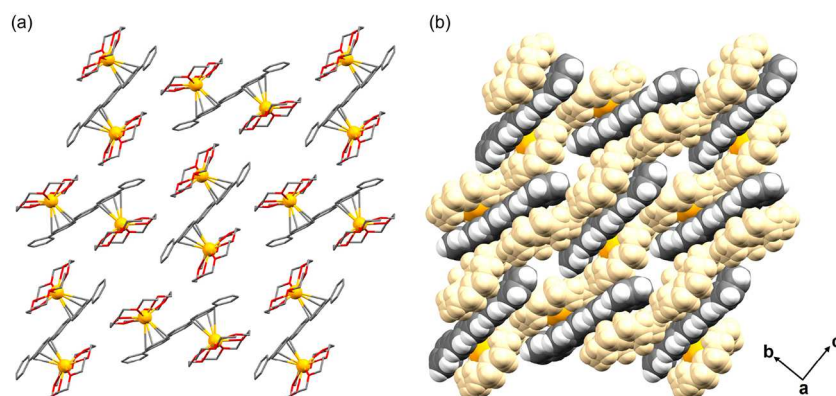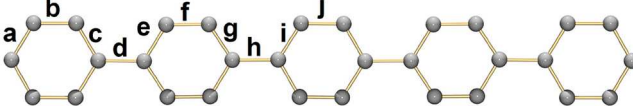similar binding mode has been observed in the doubly reduced [6]CPP and [8]CPP, with the K−C distances being slightly longer due to the curvature of these macrocycles.[72,73] The coordination environment of the K+ ion in **4** is completed by an equatorial 18-crown-6 ether (K−O$_{crown}$: 2.752(2)−2.871(2) Å) and an axial THF molecule (K−O$_{THF}$: 2.747(3) Å), with the K−C and K−O distances being comparable to those reported in the literature.[23,68,69,72−74]

In the crystal structure of **5**, there is only one independent Rb+ ion (Figure S27). Similar to **4**, the Rb+ ion is coordinated to the phenyl ring next to the central one but in an asymmetric η^6-fashion with the Rb−C distances ranging over 3.195(1)−3.574(1) Å (Figure 6). The Rb+ ion is also entrapped by an 18-crown-6 ether (Rb−O$_{crown}$: 2.755(10)−2.813(10) Å) with all Rb−C and Rb−O distances being close to those previously reported.[68,75−77]

Despite the absence of the coordinated THF molecules in **5**, similar solid-state packing patterns are observed in **4** and **5**. In both crystal structures (Figures 7 and 8), 2D layers are formed along b and c axes through C−H···π interactions between the **1**$^{2−}$ anions and 18-crown-6 ether from adjacent cationic moieties, with the contacts of 2.559(2)−2.641(2) Å and 2.737(2)−2.807(2) Å, respectively. No significant interactions are found between the adjacent layers.

***p*-Quinquephenyl Core Transformation Analysis.** The addition of two electrons leads to structural deformation of the paraphenylene core, which can be illustrated by a direct comparison of C−C bond lengths between **1** and **1**$^{2−}$ (Table 1). Taking **1**$^{2−}$ in **2** as an example, a quinoidal distortion along

Table 1. Key C−C Bond Lengths (Å) of 1 and 1$^{2−}$ in 2−5 along with a Labeling Scheme

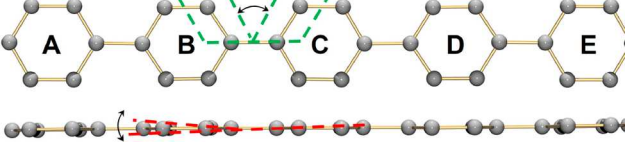| bond	**1**[40]	**2**^{a}	**3**	**4**	**5**
a	1.376(7)	1.386(13)	1.386(10)	1.398(2)	1.392(2)
b	1.386(7)	1.380(13)	1.384(10)	1.390(2)	1.387(2)
c	1.390(7)	1.415(13)	1.408(10)	1.422(2)	1.418(2)
d	1.484(7)	1.444(13)	1.465(10)	1.451(2)	1.454(2)
e	1.373(7)	1.418(13)	1.417(10)	1.427(2)	1.425(2)
f	1.379(7)	1.368(13)	1.373(10)	1.378(2)	1.376(2)
g	1.371(7)	1.432(13)	1.432(10)	1.437(2)	1.440(2)
h	1.485(7)	1.421(13)	1.426(10)	1.426(2)	1.424(2)
i	1.379(7)	1.432(13)	1.436(10)	1.438(2)	1.438(2)
j	1.380(7)	1.364(13)	1.368(10)	1.374(2)	1.371(2)

^{a}Values are averaged.

the molecular chain is observed upon chemical reduction (Figure 9). In **1**, the C−C bond lengths at **a**, **c**, **e**, and **g** range from 1.371(7) Å to 1.390(7) Å. They are slightly elongated at **a** and **c** ($\Delta_{avg.}$ = 0.015 Å) and more notably elongated at **e** and **g** ($\Delta_{avg.}$ = 0.055 Å) in **2**. Moreover, the C−C bond lengths at **b**, **f**, and **j** in **2** are gradually decreased by 0.006, 0.011, and 0.016 Å, respectively. It should be noted that the C−C bonds connecting the phenyl rings (**d** and **h**) are significantly shortened to 1.444(13) and 1.421(13) Å in **2**. These bond length alterations clearly reveal the quinoidal character and change in aromaticity of **1** upon 2-fold reduction, which is consistent with the core transformation observed in the doubly reduced [n]CPPs.[72,73]
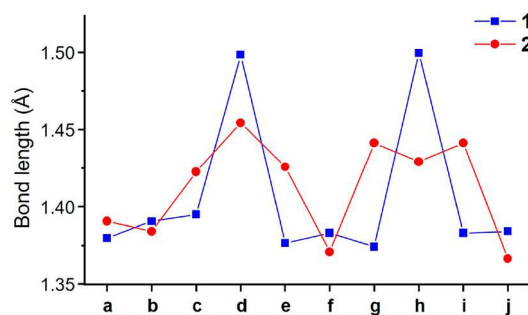
Figure 9. Comparison of C−C bond lengths in **1** and **1**$^{2−}$ in **2**.

In addition, an unusual structural distortion of the paraphenylene core is observed upon chemical reduction. Despite having free rotation around the single C−C bonds connecting six-membered rings, the neutral parent exhibits a near-planar conformation in the solid state (Table 2). In

Table 2. Selected Twisting (Green) and Bending (Red) Angles (deg) between Phenyl Rings in 1 and 1$^{2−}$ in 2−5 along with a Labeling Scheme

	angle	**1**	**2**^{a}	**3**	**4**	**5**
twisting angle^b	A−C	1.2	0.2	1.7	0.8	12.4
	B−C	0.1	4.5	9.3	1.0	0.1
	D−C	0.1	2.6	4.9	1.0	0.1
	E−C	1.2	2.4	3.7	0.8	12.4
bending angle^c	A/C	0.9	4.3	4.8	1.7	0.3
	B/C	1.1	2.6	2.1	2.1	1.1
	D/C	1.1	2.3	5.7	2.1	1.1
	E/C	0.9	2.6	4.1	1.7	0.3

^{a}Values are averaged. ^{b}Twisting angle = torsion angle of two phenyl rings perpendicular to the central axis. ^{c}Bending angle = 180° − bond angle of two phenyl rings along the central axis.

doubly reduced **1**$^{2−}$, the paraphenylene core is more distorted compared to the neutral parent. Interestingly, the phenyl rings can be either "twisted" or "bent", that is, in the same complex, the ring with a larger twisting angle usually has a smaller bending angle (e.g., 0.2° and 4.3° in **2**). In products **3−5** with direct metal coordination, the large twisting angle (or small bending angle) is observed at the rings without any metal binding (e.g., 9.3° and 2.1° in **4**); in contrast, those with metal coordination are less twisted but slightly bent (e.g., 1.0° and 2.1° in **4**).

NMR Spectroscopic Study. A careful literature search revealed that NMR spectroscopic investigation of **1** and **1**$^{2−}$ has not been reported. Therefore, a thorough NMR spectroscopic analysis of **1−5** has been carried out, targeting evaluation of the effect of 2-fold reduction and alkali metal binding. Due to poor solubility of **1** in THF at room temperature, the ^1H (Figures 10a and S9) and $^1H-^1H$ COSY (Figure S10) NMR spectra were recorded in THF-d_8 at 60 °C. Notably, the proton shifts of **1** at 60 °C are close to those at room temperature (see the Supporting Information for more details), thus they can be used for comparison with the doubly
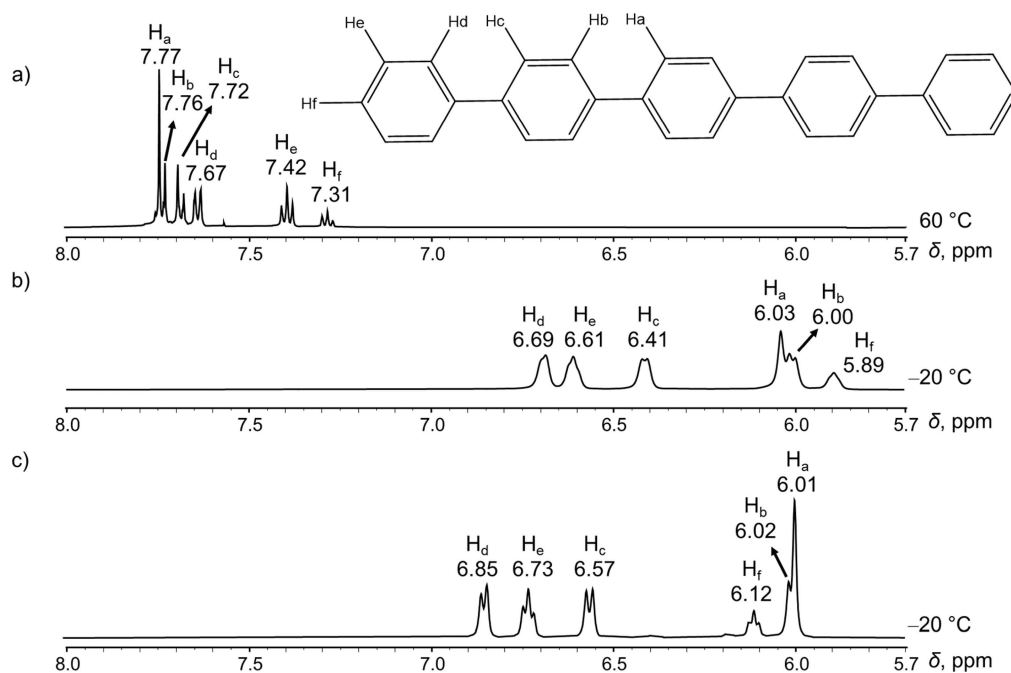
Figure 10. ^{1}H NMR spectra of (a) **1** at 60 °C, (b) **2** at −20 °C, and (c) **3** at −20 °C in THF-d_8 aromatic region.
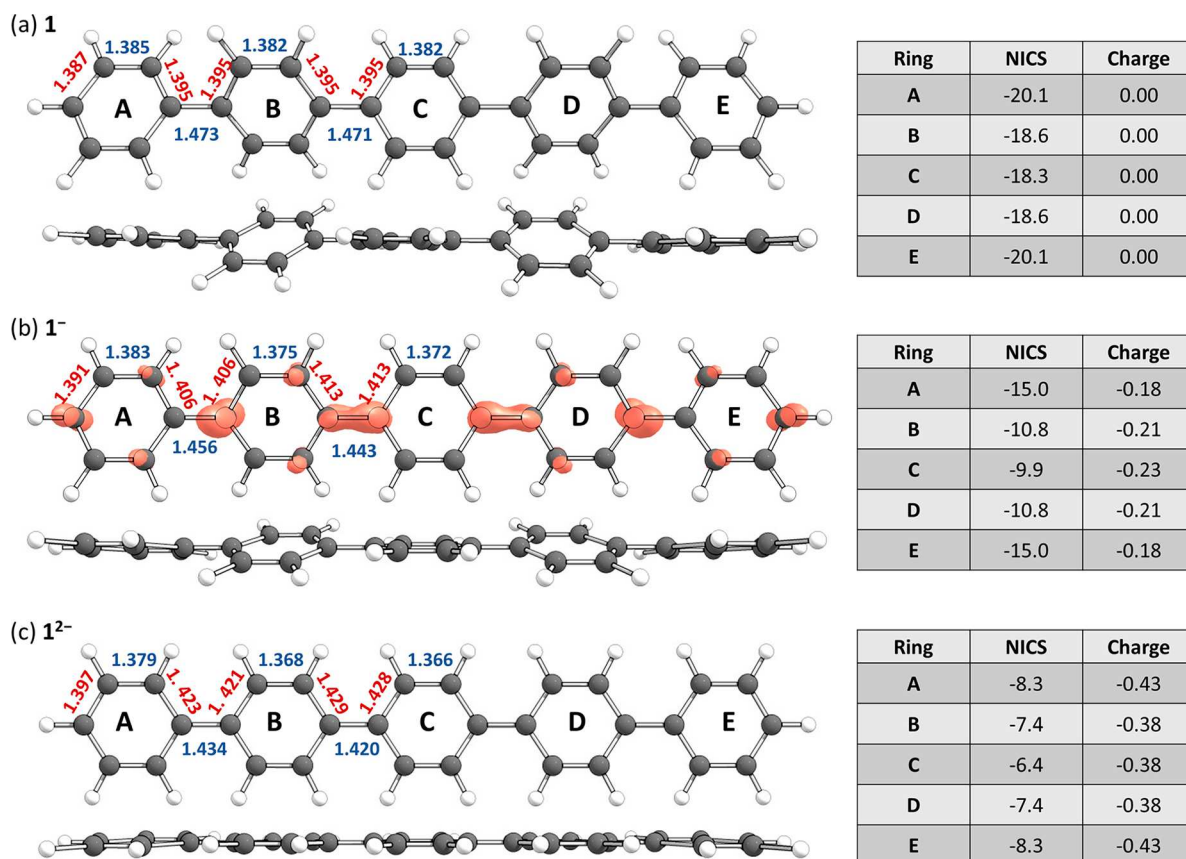
Figure 11. Front-view and side-view of the optimized geometries for (a) neutral **1**; (b) monoanion **1$^−$**; and (c) dianion **1$^{2−}$**. Selected bond lengths (in Å) are displayed for the structures. Blue denotes bonds that are parallel to the main axis of the molecule; red denotes bonds that are not parallel to the main axis of the molecule. NICS(1.7)$_{ZZ}$ values (in ppm) and Loewdin partial charges for each ring are provided in a table beside each compound. For the radical anion (b), the spin density is plotted at an isosurface value of $\alpha = 0.005$.

reduced species. In the ^{1}H NMR spectra of **2** and **3** (Figures 10b,c and S11−S16), the protons of **1$^{2−}$** are notably shifted upfield compared to the neutral state, consistent with a combined effect of two-electron addition and aromaticity reduction in the quinquephenyl core. The largest shift found around ring C (1.7 ppm) is still smaller than that observed in

(a) **2**

Ring	NICS	Charge
A	-11.8	-0.29
B	-8.5	-0.34
C	-7.2	-0.33
D	-9.4	-0.32
E	-12.2	-0.27

(c) **4**

Ring	NICS	Charge
A	-14.1	-0.26
B	-7.6	-0.36
C	-7.0	-0.42
D	-7.6	-0.36
E	-14.1	-0.26

(b) **3**

Ring	NICS	Charge
A	-17.0	-0.14
B	-11.6	-0.24
C	-1.2	-0.40
D	-9.0	-0.39
E	-15.0	-0.25

(d) **5**

Ring	NICS	Charge
A	-15.1	-0.21
B	-6.7	-0.48
C	-8.4	-0.38
D	-6.6	-0.48
E	-15.1	-0.21
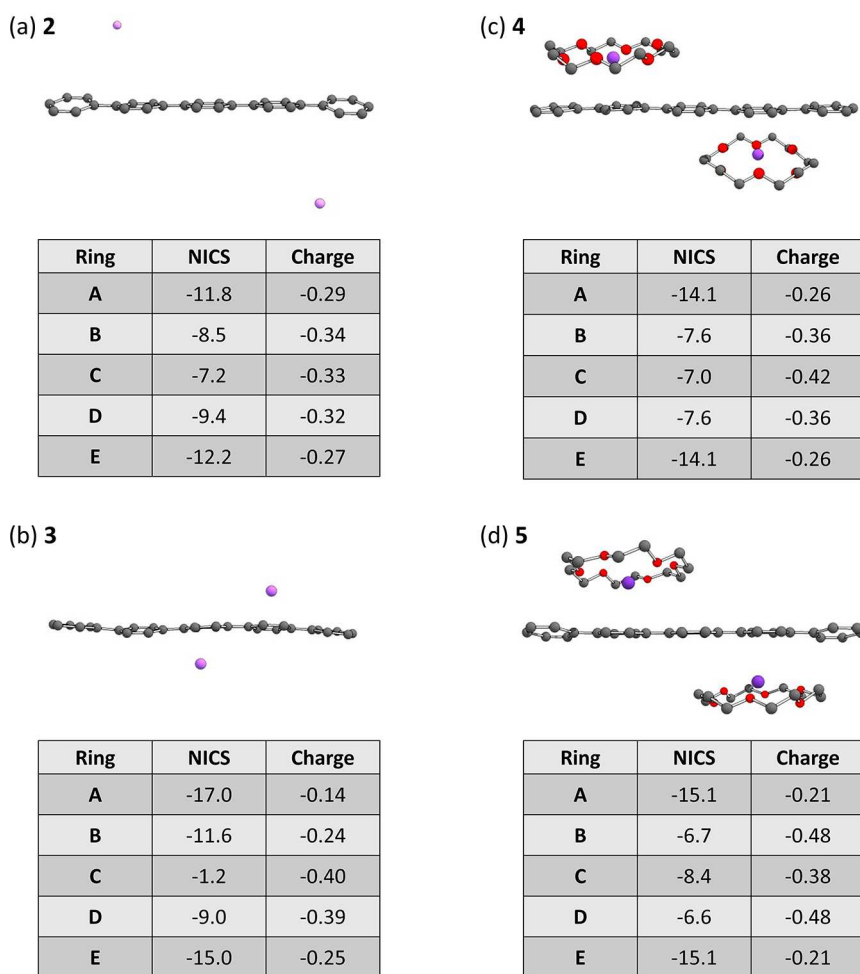
Figure 12. NICS(1.7)$_{ZZ}$ values and partial charges for the individual rings in structures (a) **2** (averaged values), (b) **3**, (c) **4**, and (d) **5**. The rings are denoted A−E, reading from the left-hand side of *p*-quinquephenyl. To clarify the relative position of the metal in each structure, a side view of the computed structures are provided as well, with solvent molecules and hydrogen atoms removed for better visibility.

[*n*]cycloparaphenylene (2.2 ppm), where the quinoidal distortion upon 2-fold reduction is symmetric and more pronounced.[73] Taking **2** as an example, the H$_a$ and H$_b$ proton signals are shifted upfield to 6.03 and 6.00 ppm in comparison to 7.77 and 7.76 ppm in the neutral state. Doublets H$_c$ and H$_d$ are shifted to 6.41 and 6.69 ppm in contrast to 7.72 and 7.67 ppm, respectively. Finally, triplets H$_e$ and H$_f$ are shifted to 6.61 and 5.89 ppm in comparison to 7.42 and 7.31 ppm, respectively. Similarly, H$_a$ and H$_b$ in **3** are comparable, and all other proton shifts vary by 0.12−0.23 ppm. This is particularly apparent in the triplet corresponding to H$_f$ which shifts by 0.23 ppm and has different positioning in **2** and **3**. Considering the nature of the doubly reduced product, the signals of $\mathbf{1^{2-}}$ in **2** are shifted slightly downfield than those for complexes **4** and **5** (see the Supporting Information for more details), but shifted slightly more upfield compared to **3**, which may stem from weaker interactions of Na$^+$ ions to the doubly reduced quinquephenyl core in solution. Recently, we investigated the reduction of pentacene through NMR spectroscopy[68] and revealed that the signals of the doubly reduced pentacene shift considerably (up to 4.46 ppm) compared to neutral parent. This is a stark contrast to the solution behavior of *p*-quinquephenyl and its doubly reduced state, where the proton signals are shifted to a far lesser extent.

Computational Investigation. To better understand the behavior of the parent *p*-quinquephenyl (**1**), its dianion ($\mathbf{1^{2-}}$), and the complexes of the dianion with alkali metals, we performed a computational investigation. In our study, we focused on the geometric, electronic, and aromatic changes the hydrocarbon system undergoes due to reduction and complexation.

To begin, we characterized the "naked" parent, **1**. In contrast to the planar geometry observed in the crystal structure, the fully optimized gas-phase neutral system adopts a nonplanar structure, in which the neighboring rings are twisted relative to each other (i.e., with a "biphenyl angle"). The driving force for such twisting is usually attributed to reduction of steric hindrance. However, it may also have an electronic component: this arrangement allows breaking of the conjugation between adjacent rings to a certain extent, which enables them each to sustain local ring currents (i.e., local aromaticity). Hence, it is likely that the planarity seen in the crystal structure is caused by packing forces. Indeed, the NICS(1.7)$_{ZZ}$ values of the individual rings in the neutral *p*-quinquephenyl indicate that each of the rings has marked aromatic character (approximately −20 ppm, or 91% of benzene; NICS(1.7)$_{ZZ}$ = −22 ppm for benzene at the same level of theory) and the total value for the molecule is ΣNICS(1.7)$_{ZZ}$ = −95.7 ppm. There are very slight differences

between the six-membered rings along the core (see table in Figure 11a), with the middle ring (ring C) displaying the least negative values and the external rings (rings A/E) displaying the most negative values. These observations are in agreement with a previous investigation of polyphenyl oligomers and their aromatic behavior.[78]

Upon reduction to the radical monoanion, the dihedral angles decrease as the molecule tends more toward planarity (see side view in Figure 11b). In addition, the characteristic geometric features of a quinoidal system appear: shortening of the bond lengths along the backbone of the polycyclic system (bonds **b**, **d**, **f**, **h**, and **j** in Table 1, shown in blue in Figure 11) and elongation of the bond lengths at the alternating positions (bonds **a**, **c**, **e**, **g**, and **i** in Table 1, shown in red in Figure 11). The electronic structure analysis confirms this transformation. There is a loss of aromaticity in all of the rings, as seen from the total value of ΣNICS(1.7)$_{ZZ}$ = -64.1 ppm, and the individual NICS(1.7)$_{ZZ}$ values decreasing (in absolute value) to range between -10 ppm to -16 ppm (45–73% of benzene). The ACID plot (Figure S29) also shows that the individual ring currents of the neutral species change to a molecular current along the length of the core. As with the neutral system, the strongest diatropicity is in the outer rings and the weakest is in the center ring, albeit the differences are quite small. An opposite trend is observed for the partial charges, whereby there is slightly greater negative charge accumulation in the center rings than in the external rings. This is somewhat similar to the monoreduced triphenylene systems studied previously,[77] in which six-membered rings with higher negative charge displayed stronger antiaromaticity. Here, we observe that the rings with more charge are less aromatic. Overall, the changes in aromaticity, together with the spin-density distribution (Figure 11b), corroborate the quinoidal character of the monoanion.

Following the second reduction to afford the "naked" dianion, the core becomes almost completely planar, and the bond alternation becomes even more pronounced (see side view and detailed bond lengths in Figure 11c). The aromaticity of the system is also further reduced, to ΣNICS(1.7)$_{ZZ}$ = -37.7 ppm, with individual NICS(1.7)$_{ZZ}$ values ranging between -6 and -8 ppm (27–36% of benzene). The ACID plot (Figure S29) also shows an increase in the current density along the backbone of the molecule. Thus, the computational results indicate that the quinoidal character is strengthened by the second reduction. Interestingly, as opposed to the radical monoanion, in the dianion the partial negative charge is larger in the outer rings. A plausible explanation is that the stronger repulsive charge interactions in the doubly reduced core are mitigated by separation of the charges over the length of the molecule.

With a better understanding of the behavior of *p*-quinquephenyl upon addition of one and two electrons, we now turn to analyzing the effects of complexation to the various alkali metal cations. As mentioned above, in **2** there is no direct complexation of the Li$^+$ cations to the dianionic core; instead the {Li(THF)$_4$}$^+$ species engage in multiple C−H···π interactions with the surface of **1^{2-}** anions (Figure S21). Based on the crystal structure, we identified five distinct types of such interactions and calculated the partial charges and NICS(1.7)$_{ZZ}$ for all. The individual systems generally display very similar features; thus we report here the averaged values obtained from these five models. The results for different models are reported in the Supporting Information. Despite

the lack of direct complexation, there is an apparent shift in charge distribution and aromaticity of the hydrocarbon scaffold, most likely due to the aforementioned C−H···π interactions. The average charge on the hydrocarbon core is reduced from -2 to -1.56, which indicates charge transfer to the solvated Li$^+$ ion. We observe that the loss of negative charge is linked to a reversion to stronger aromaticity, which is seen both in the averaged global value of ΣNICS(1.7)$_{ZZ}$ = -49.0 ppm and in the individual values (e.g., the accumulated charge in ring E is decreased from -0.43 to -0.27 and its NICS(1.7)$_{ZZ}$ value decreases from -8.3 to -12.1 ppm) (Figure 12).

Unsurprisingly, the direct complexation of Na$^+$ to afford complex **3** shows more pronounced effects. The cationic metal centers are bound to the internal six-membered rings (in this case, rings C and D). The partial charges in the outer rings are further reduced, and the rings closest to the metal centers again show the largest charge accumulation. Concurrently, the aromatic character of the rings shift in the same trend as before: the outer rings, which have the least charge, show the greatest diatropicity, reaching values as low as NICS(1.7)$_{ZZ}$ = -15.0 ppm; the inner rings with the most charge reach values as high as NICS(1.7)$_{ZZ}$ = -1.0 ppm (essentially nonaromatic). The total charge of the organic system is -1.42, which indicates a substantial shift of the negative charge to the metal centers. This is likely enabled by the closer interaction between the alkali metal cations and the hydrocarbon core. The further reduction in charge aligns well with the lower total aromaticity of ΣNICS(1.7)$_{ZZ}$ = -53.9 ppm.

Complexes **4** and **5**, formed by complexation of K$^+$ and Rb$^+$ ions to **1^{2-}**, respectively, show somewhat different structural patterns. In these cases, the cations are bound to rings B and D, rather than to adjacent rings B and C/C and D. Here, as well, the partial negative charge is largest on the rings serving as binding sites to the metal ions. However, it appears that the charge transfer between the dianionic core and the cationic metal centers is not as efficient, leaving charges of -1.66 and -1.76 on the hydrocarbon components in **4** and **5**, respectively. This is perhaps due to the stabilization of the metal centers by the crown ethers, which provides them with a smaller effective positive charge and poorer contact with the **1^{2-}** core. A similar metal ion size-dependent trend was observed for the complexation of the monoreduced triphenylene, whereby charge transfer was more effective for K$^+$, but less so for Rb$^+$ and Cs$^+$.[77] The less efficient charge transfer results in decreased aromaticity, as seen in the values of ΣNICS(1.7)$_{ZZ}$ = -50.3 ppm and ΣNICS(1.7)$_{ZZ}$ = -51.8 ppm for **4** and **5**, respectively. The trends for the individual rings also remain the same: The rings with greater negative charge display weaker diatropicity, and those with less charge display stronger diatropicity.

In summary, the computational results show that the neutral *p*-quinquephenyl comprises a series of strongly aromatic rings. Addition of one electron to the system causes a reduction in the aromatic character and the adoption of a quinoidal structure, which can be seen in the geometric and electronic properties of the system. Introduction of a second electron leads to more pronounced quinoidal characteristics, along with further reduction of aromaticity. Complexation to the various alkali metal cations allows the doubly-reduced anion to relieve some of the excess negative charge and, in doing so, regain some of its aromatic character. This interpretation is supported by the excellent agreement between ΣNICS(1.7)$_{ZZ}$ and the

total charge on the hydrocarbon system (Figure 13, R^2 = 0.9758). Moreover, we find that this effect is site-dependent:
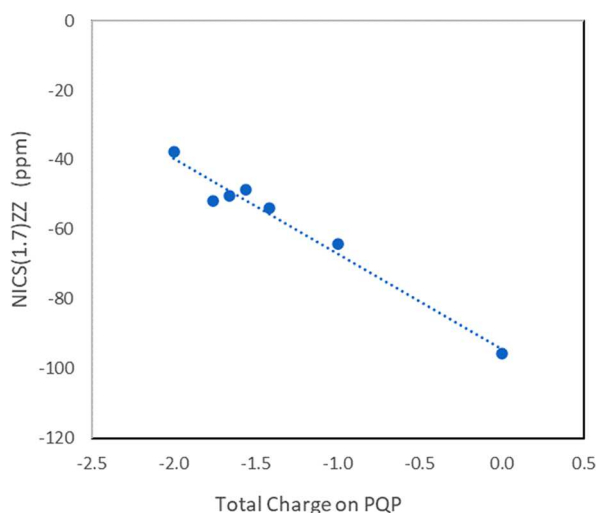
Figure 13. Scatter plot of the $\Sigma NICS(1.7)_{ZZ}$ against the total charge for the *p*-quinquephenyl system in all of the states and complexes studied in this report (i.e., structures **1**, **1⁻**, **1²⁻**, **2**, **3**, **4**, and **5**). R^2 = 0.9713. The value used for **2** is the average of the five models.

The rings that serve as binding sites to the metal centers retain the greatest negative charge and are least aromatic; the farther rings have less charge and, accordingly, regain more of their aromatic character. These conclusions are further corroborated by the good linear correlation between the partial charge of the individual rings and its $NICS(1.7)_{ZZ}$ value (see the Supporting Information).

CONCLUSION

Using chemical reduction with different alkali metals, we revealed that *p*-quinquephenyl, **1**, functions as a two-electron acceptor to afford the doubly reduced anion, **1²⁻**. Several products of **1²⁻** have been isolated and crystallographically characterized to illustrate that alkali metal ion binding differs for light (Li⁺ vs Na⁺) and heavy (K⁺ and Rb⁺) congeners. The analysis of crystal structures also detected a notable quinoidal core transformation of the dianion. The ¹H NMR investigation of *p*-quinquephenyl further supported the reduction in aromaticity illustrated by notable upfield shifts of all protons upon 2-fold electron addition.

Furthermore, our computational analysis characterized the *p*-quinquephenyl system in all the states relevant to the experimental studies: neutral, anionic, dianionic, and complexed to various alkali metal cations. We observed that reduction of the aromatic scaffold leads to an increase in quinoidal character and a concurrent decrease in aromatic character, which is exacerbated upon the second reduction step. This apparent relationship between the charge and aromaticity was supported by the analysis of complexed systems. Upon complexation to the alkali metal cations, the negative charge of the *p*-quinquephenyl dianion is partially alleviated and some of the aromatic character is regained. The series of alkali metals reveals a well-behaved correlation between the extent of charge shift and regaining of aromaticity for **1²⁻**. Interestingly, the Li⁺ ion fits well within this correlation, even though the mechanism of charge transfer in

this case is through C−H⋯π intermolecular interactions and not due to direct complexation.

Overall, the series of alkali-metal salts prepared in this work provides the first crystallographically characterized examples of the doubly reduced *p*-quinquephenyl. These products could be now utilized in ligand metathesis reactions providing access to new d- and f-metal complexes and expanding their chemistry and applications.

EXPERIMENTAL SECTION

Materials and Methods. All manipulations were carried out using break-and-seal[79] and glovebox techniques under an atmosphere of argon. Tetrahydrofuran (THF) and hexanes (Sigma-Aldrich) were dried over Na/benzophenone and distilled prior to use. THF-d_8 (≥99.5 atom %D, Sigma-Aldrich) was dried over NaK₂ alloy and vacuum-transferred. *p*-Quinquephenyl (**1**) (99%) was purchased from TCI and sublimed at 280 °C prior to use. Lithium (99.9%), sodium (99.9%), potassium (98%), rubidium (99.6%), and 18-crown-6 ether (99%) were purchased from Sigma-Aldrich and used as received. The UV−vis absorption spectra were recorded on a Thermo Scientific Evolution 201 UV−visible Spectrophotometer. The ¹H and ¹³C NMR spectra were measured using Bruker Ascend-500 spectrometer (500 MHz for ¹H and 126 MHz for ¹³C) and referenced to the resonances of THF-d_8. The low-temperature NMR experiment was controlled by a Cryo Diffusion cryogenic tank probe, and liquid N₂ was used as a cooling source. The extreme air- and moisture sensitivity of crystals **2**−**5**, along with the presence of loosely-bound THF molecules, prevented obtaining elemental analysis data.

[Li⁺(THF)₄]₂[(1²⁻)]·0.4THF (2·0.4THF). THF (1.5 mL) was added to a custom-built glass system containing **1** (2.0 mg, 0.005 mmol) and excess Li metal (0.5 mg, 0.070 mmol). The mixture was allowed to stir under argon at 25 °C for 24 h in a closed system. The initial color of the suspension was off-white (neutral ligand), and it changed to light pink after 10 min and deepened to a deep purple-red after 20 min. The suspension was filtered, and the purple-blue filtrate was layered with 2.0 mL of hexanes. The ampule was sealed and placed at 5 °C. Purple-black plates were deposited after 7 days. Yield: 1.0 mg, 50%. ¹H NMR (THF-d_8, ppm, −40 °C): δ 5.86−5.92 (2H, **1²⁻**), 5.97−6.08 (8H, **1²⁻**), 6.37−6.45 (4H, **1²⁻**), 6.58−6.64 (4H, **1²⁻**), 6.66−6.73 (4H, **1²⁻**) UV−vis (THF, nm): λ_{max} 490.

[{Na⁺(THF)₃}₂(1²⁻)] (3). THF (1.3 mL) was added to a custom-built glass system containing **1** (2.0 mg, 0.005 mmol) and excess Na metal (5.0 mg, 0.22 mmol). The mixture was allowed to stir under argon at 25 °C for 8 h in a closed system. The initial color of the suspension was off-white (neutral ligand), and it changed to light pink after 5 min and deepened to dark purple after 15 min. The suspension was filtered, and the purple-blue filtrate was layered with 2.0 mL of hexanes. The ampule was sealed and placed at 5 °C. Black-red blocks were deposited after 7 days. Yield: 1.5 mg, 75%. ¹H NMR (THF-d_8, ppm, −20 °C): δ 5.98−6.05 (8H, **1²⁻**), 6.09−6.14 (2H, **1²⁻**), 6.54−6.60 (4H, **1²⁻**), 6.70−6.77 (4H, **1²⁻**), 6.83−6.88 (4H, **1²⁻**). UV−vis (THF, nm): λ_{max} 321, 392.

[{K⁺(18-crown-6)(THF)}₂(1²⁻)] (4). THF (1.8 mL) was added to a custom-built glass system containing **1** (4.0 mg, 0.01 mmol), and excess K metal (5.0 mg, 0.130 mmol). The mixture was allowed to stir under argon at 25 °C for 6 h in a closed system. The initial color of the suspension was off-white (neutral ligand), and it changed to light pink after 2 min and deepened to dark brown after 10 min. The suspension was filtered, and the purple-blue filtrate was layered with 2.0 mL of hexanes containing 18-crown-6 (15 mg, 0.056 mmol). The ampule was sealed and placed at 5 °C. Black blocks were deposited after 7 days. Yield: 1.5 mg, 38%. UV−vis (THF, nm): λ_{max} 328.

[{Rb⁺(18-crown-6)}₂(1²⁻)] (5). THF (1.8 mL) was added to a custom-built glass system containing **1** (4.0 mg, 0.01 mmol), and excess Rb metal (10 mg, 0.118 mmol). The mixture was allowed to stir under argon at 25 °C for 4 h in a closed system. The initial color of the suspension was off-white (neutral ligand), and it changed to light pink after 1 min and deepened to dark brown after 5 min. The suspension was filtered, and the brown filtrate was layered with 2.0

mL of hexanes containing 18-crown-6 (15 mg, 0.056 mmol). The ampule was sealed and placed at 5 °C. Brown blocks were deposited after 7 days. Yield: 1.3 mg, 33%. UV–vis (THF, nm): λ_{max} 321.

Crystal Structure Determination and Refinement. Data collections of **2**, **3**, and **5** were performed on a Bruker VENTURE system equipped with a PHOTON 100 CMOS detector, a Mo-target fine-focus X-ray source (λ = 0.71073 Å), and a graphite monochromator. The data were collected at 100(2) K (Oxford Cryosystems CRYOSTREAM 700), 50 kV, and 30 mA with an appropriate 0.5° ω scan strategy. Data collection of **4** was performed at 100(2) K on a Huber Kappa system with a DECTRIS PILATUS3 × 2M(CdTe) pixel array detector using ϕ scans (synchrotron radiation at λ = 0.49594 Å) located at the Advanced Photon Source, Argonne National Laboratory (NSF's ChemMatCARS, Sector 15, Beamline 15-ID-D).

All data sets' reduction and integration were performed with the Bruker software package SAINT (version 8.38A).[80] Data were corrected for absorption effects using the empirical methods as implemented in SADABS (version 2016/2).[81] The structures were solved by SHELXT (version 2018/2)[82] and refined by full-matrix least-squares procedures using the Bruker SHELXTL (version 2019/2)[83] software package through the OLEX2 graphical interface.[84] All non-hydrogen atoms, including those in disordered parts, were refined anisotropically. Hydrogen atoms were included in idealized positions for structure factor calculations with $U_{iso}(H) = 1.2\ U_{eq}(C)$. More crystallographic details and structure refinement (Table S2) as well as ORTEP drawings and solid-state packing are shown in the Supporting Information.

Computational Details. All calculations were performed with the ORCA 5.0.3 software package[85] using the PBE0[86,87] functional and the def2-TZVPD[88,89] basis set. Dispersion effects were accounted for using Grimme's D3 correction with Becke–Johnson damping.[90,91] Specific computational keywords are detailed in the sample input files in the Supporting Information. For the parent *p*-quinquephenyl structures (neutral, radical anion, and dianion), full optimizations were performed, and frequency calculations confirmed the optimized structures to be real minima (i.e., N_{imag} = 0). For products **2**, **3**, **4**, and **5**, constrained optimizations were performed, in which only the hydrogen coordinates were optimized on the crystal-structure coordinates; all other atoms were kept frozen. XYZ coordinate files for the NICS calculations[92,93] were generated with the AROMA package.[94] ACID plots[95,96] were generated with the Gaussian 09 suite of programs, revision D.01.[97] The partial charges discussed in the text are Loewdin charges calculated for the carbon atoms with the bonded hydrogens. To obtain partial charges for each ring, the values were summed over all carbons within each ring.

■ ASSOCIATED CONTENT

ⓈⅠ Supporting Information

The Supporting Information is available free of charge at https://pubs.acs.org/doi/10.1021/acs.organomet.2c00583.

> X-ray structural details, UV–vis and NMR spectra, as well as computational data (PDF)
>
> Coordinate files for the NICS calculations (XYZ)

Accession Codes

CCDC 2218890–2218893 contain the supplementary crystallographic data for this paper. These data can be obtained free of charge via www.ccdc.cam.ac.uk/data_request/cif, or by emailing data_request@ccdc.cam.ac.uk, or by contacting The Cambridge Crystallographic Data Centre, 12 Union Road, Cambridge CB2 1EZ, UK; fax: +44 1223 336033.

■ AUTHOR INFORMATION

Corresponding Authors

Marina A. Petrukhina − *Department of Chemistry, University at Albany, State University of New York, Albany, New York 12222, United States;* ◎ orcid.org/0000-0003-0221-7900; Email: mpetrukhina@albany.edu

Renana Gershoni-Poranne − *Schulich Faculty of Chemistry, Technion — Israel Institute of Technology, Technion City, Haifa 32000, Israel;* ◎ orcid.org/0000-0002-2233-6854; Email: rporanne@technion.ac.il

Authors

Matthew Pennachio − *Department of Chemistry, University at Albany, State University of New York, Albany, New York 12222, United States*

Zheng Zhou − *Department of Chemistry, University at Albany, State University of New York, Albany, New York 12222, United States; School of Materials Science and Engineering, Tongji University, Shanghai 201804, China*

Zheng Wei − *Department of Chemistry, University at Albany, State University of New York, Albany, New York 12222, United States*

Alexandra Tsybizova − *Laboratory for Organic Chemistry, ETH Zurich, Zurich 8092, Switzerland*

Complete contact information is available at:
https://pubs.acs.org/10.1021/acs.organomet.2c00583

Notes

The authors declare no competing financial interest.

■ REFERENCES

(1) Benshafrut, R.; Shabtai, E.; Rabinovitz, M.; Scott, L. T. *π*-Conjugated Anions: From Carbon-Rich Anions to Charged Carbon Allotropes. *Eur. J. Org. Chem.* **2000**, *2000*, 1091−1106.

(2) Sternfeld, T.; Rabinovitz, M. Reduction of Carbon-rich Compounds. In *Carbon-Rich Compounds*; Haley, M. M.; Tykwinski, R. R., Eds.; Wiley: Weinheim, Germany, 2006; pp 566−623.

(3) Eisenberg, D.; Shenhar, R. Polyarene Anions: Interplay between Theory and Experiment. *WIREs: Comput. Mol. Sci.* **2012**, *2*, 525−547.

(4) Tzirakis, M. D.; Orfanopoulos, M. Radical Reactions of Fullerenes: From Synthetic Organic Chemistry to Materials Science and Biology. *Chem. Rev.* **2013**, *113*, 5262−5321.

(5) Zabula, A. V.; Petrukhina, M. A. Structural Perspective on Aggregation of Alkali Metal Ions with Charged Planar and Curved Carbon *π*-Surfaces. *Adv. Organomet. Chem.* **2013**, *61*, 375−462.

(6) Bock, H.; Gharagozloo-Hubmann, K.; Sievert, M.; Prisner, T.; Havlas, Z. Single Crystals of an Ionic Anthracene Aggregate with a Triplet Ground State. *Nature* **2000**, *404*, 267−269.

(7) Ayalon, A.; Sygula, A.; Cheng, P.-C.; Rabinovitz, M.; Rabideau, P. W.; Scott, L. T. Stable High-Order Molecular Sandwiches: Hydrocarbon Polyanion Pairs with Multiple Lithium Ions Inside and Out. *Science* **1994**, *265*, 1065−1067.

(8) Treitel, N.; Sheradsky, T.; Peng, L.; Scott, L. T.; Rabinovitz, M. $C_{30}H_{12}{}^{6-}$: Self-Aggregation, High Charge Density, and Pyramidaliza-

tion in a Supramolecular Structure of a Supercharged Hemifullerene. *Angew. Chem. Int. Ed* **2006**, *45*, 3273−3277.

(9) Eisenberg, D.; Jackson, E. A.; Quimby, J. M.; Scott, L. T.; Shenhar, R. The Bicorannulenyl Dianion: A Charged Overcrowded Ethylene. *Angew. Chem. Int. Ed* **2010**, *49*, 7538−7542.

(10) Zabula, A. V.; Filatov, A. S.; Spisak, S. N.; Rogachev, A. Yu.; Petrukhina, M. A. A Main Group Metal Sandwich: Five Lithium Cations Jammed Between Two Corannulene Tetraanion Decks. *Science* **2011**, *333*, 1008−1011.

(11) Zabula, A. V.; Filatov, A. S.; Xia, J.; Jasti, R.; Petrukhina, M. A. Tightening of the Nanobelt upon Multielectron Reduction. *Angew. Chem. Int. Ed* **2013**, *52*, 5033−5036.

(12) Spisak, S. N.; Wei, Z.; O'Neil, N. J.; Rogachev, A. Yu.; Amaya, T.; Hirao, T.; Petrukhina, M. A. Convex and Concave Encapsulation of Multiple Potassium Ions by Sumanenyl Anions. *J. Am. Chem. Soc.* **2015**, *137*, 9768−9771.

(13) Wombacher, T.; Goddard, R.; Lehmann, C. W.; Schneider, J. J. Complete Charge Separation Provoked by Full Cation Encapsulation in the Radical Mono- and Di-anions of 5,6:11,12-di-*o*-Phenylene-tetracene. *Dalton Trans* **2018**, *47*, 10874−10883.

(14) Zabula, A. V.; Spisak, S. N.; Filatov, A. S.; Rogachev, A. Yu.; Petrukhina, M. A. Record Alkali Metal Intercalation by Highly Charged Corannulene. *Acc. Chem. Res.* **2018**, *51*, 1541−1549.

(15) Zhou, Z.; Spisak, S. N.; Xu, Q.; Rogachev, A. Yu.; Wei, Z.; Marcaccio, M.; Petrukhina, M. A. Fusing a Planar Group to a π-Bowl: Electronic and Molecular Structure, Aromaticity and Solid-State Packing of Naphthocorannulene and its Anions. *Chem. - Eur. J.* **2018**, *24*, 3455−3463.

(16) Spisak, S. N.; Bühringer, M. U.; Wei, Z.; Zhou, Z.; Tykwinski, R. R.; Petrukhina, M. A. Structural and Electronic Effects of Stepwise Reduction of a Tetraaryl[3]Cumulene. *Angew. Chem. Int. Ed* **2019**, *58*, 2023−2028.

(17) Zhou, Z.; Wei, Z.; Tokimaru, Y.; Ito, S.; Nozaki, K.; Petrukhina, M. A. Stepwise Reduction of Azapentabenzocorannulene. *Angew. Chem. Int. Ed* **2019**, *58*, 12107−12111.

(18) Zhou, Z.; Wang, X.-Y.; Wei, Z.; Müllen, K.; Petrukhina, M. A. Charging OBO-Fused Double [5]Helicene with Electrons. *Angew. Chem. Int. Ed* **2019**, *58*, 14969−14973.

(19) Bock, H.; Havlas, Z.; Gharagozloo-Hubmann, K.; Sievert, M. The Li⁺-Initiated Twofold Dehydrogenation and C−C Bond Formation of Hexaphenylbenzene to the Dilithium Salt of the 9,10-Diphenyltetrabenz[*a,c,h,j*]anthracene Dianion. *Angew. Chem. Int. Ed* **1999**, *38*, 2240−2243.

(20) Bock, H.; Sievert, M.; Bogdan, C. L.; Kolbesen, B. O.; Wittershagen, A. Biphenylene Ring Expansion by a (H₃C)₂Si Link from Silicone Grease As Proven by the Crystal Structures of [(Sodium⁺[2.2.1]cryptand)(9,9-dimethylsilafluorene•⁻)] as well as [Sodium⁺(triglyme)₂(biphenylene•⁻)] and by Total-Reflection X-ray Fluorescence Spectrometry (TXRF)¹. *Organometallics* **1999**, *18*, 2387−2389.

(21) Zhou, Z.; Kawade, R. K.; Wei, Z.; Kuriakose, F.; Üngör, Ö.; Jo, M.; Shatruk, M.; Gershoni-Poranne, R.; Petrukhina, M. A.; Alabugin, I. V. Negative Charge as a Lens for Concentrating Antiaromaticity: Using a Pentagonal "Defect" and Helicene Strain for Cyclizations. *Angew. Chem. Int. Ed* **2020**, *59*, 1256−1262.

(22) Zhou, Z.; Zhu, Y.; Wei, Z.; Bergner, J.; Neiß, C.; Doloczki, S.; Görling, A.; Kivala, M.; Petrukhina, M. A. Reversible Structural Rearrangement of π-Expanded Cyclooctatetraene upon Two-Fold Reduction with Alkali Metals. *Chem. Commun.* **2022**, *58*, 3206−3209.

(23) Zhou, Z.; Egger, D. T.; Hu, C.; Pennachio, M.; Wei, Z.; Kawade, R. K.; Üngör, Ö.; Gershoni-Poranne, R.; Petrukhina, M. A.; Alabugin, I. V. Localized Antiaromaticity Hotspot Drives Reductive Dehydrogenative Cyclizations in Bis- and Mono-Helicenes. *J. Am. Chem. Soc.* **2022**, *144*, 12321−12338.

(24) Aprahamian, I.; Hoffman, R. E.; Sheradsky, T.; Preda, D. V.; Bancu, M.; Scott, L. T.; Rabinovitz, M. A Four-Step Alternating Reductive Dimerization/Bond Cleavage of Indenocorannulene. *Angew. Chem. Int. Ed* **2002**, *41*, 1712−1715.

(25) Aprahamian, I.; Preda, D. V.; Bancu, M.; Belanger, A. P.; Sheradsky, T.; Scott, L. T.; Rabinovitz, M. Reduction of Bowl-Shaped Hydrocarbons: Dianions and Tetraanions of Annelated Corannulenes. *J. Org. Chem.* **2006**, *71*, 290−298.

(26) Spisak, S. N.; Zabula, A. V.; Alkan, M.; Filatov, A. S.; Rogachev, A. Yu.; Petrukhina, M. A. Site-Directed Dimerization of Bowl-Shaped Radical Anions to Form a σ-Bonded Dibenzocorannulene Dimer. *Angew. Chem. Int. Ed* **2018**, *57*, 6171−6175.

(27) Rogachev, A. Yu.; Alkan, M.; Li, J.; Liu, S.; Spisak, S. N.; Filatov, A. S.; Petrukhina, M. A. Mono-reduced Corannulene: To Couple and Not to Couple in One Crystal. *Chem. - Eur. J.* **2019**, *25*, 14140−14147.

(28) Kubozono, Y.; Mitamura, H.; Lee, X.; He, X.; Yamanari, Y.; Takahashi, Y.; Suzuki, Y.; Kaji, Y.; Eguchi, R.; Akaike, K.; Kambe, T.; Okamoto, H.; Fujiwara, A.; Kato, T.; Kosugi, T.; Aoki, H. Metal-Intercalated Aromatic Hydrocarbons: A New Class of Carbon-Based Superconductors. *Phys. Chem. Chem. Phys.* **2011**, *13*, 16476−16493.

(29) Garst, J. F. Electron Transfer, Naphthalene Radical Anion, and Alkyl Halides. *Acc. Chem. Res.* **1971**, *4*, 400−406.

(30) García-Gallastegui, A.; Obieta, I.; Bustero, I.; Imbuluzqueta, G.; Arbiol, J.; Miranda, J. I.; Aizpurua, J. M. Reductive Functionalization of Single-Walled Carbon Nanotubes with Lithium Metal Catalyzed by Electron Carrier Additives. *Chem. Mater.* **2008**, *20*, 4433−4438.

(31) Manzetti, S. Chemical and Electronic Properties of Polycyclic Aromatic Hydrocarbons: A Review. In *Handbook of Polycyclic Aromatic Hydrocarbons*; Bandeira, G. C.; Meneses, H. E., Eds.; Nova Science, 2011; pp 423−435.

(32) Wang, S.; Yata, S.; Nagano, J.; Okano, Y.; Kinoshita, H.; Kikuta, H.; Yamabe, T. A New Carbonaceous Material with Large Capacity and High Efficiency for Rechargeable Li-Ion Batteries. *J. Electrochem. Soc.* **2000**, *147*, 2498.

(33) Friedlein, R.; Crispin, X.; Salaneck, W. R. Molecular Parameters Controlling the Energy Storage Capability of Lithium Polyaromatic Hydrocarbon Intercalation Compounds. *J. Power Sources* **2004**, *129*, 29−33.

(34) Grimsdale, A. C.; Wu, J.; Müllen, K. New Carbon-Rich Materials for Electronics, Lithium Battery, and Hydrogen Storage Applications. *Chem. Commun.* **2005**, 2197−2204.

(35) Bachman, J. C.; Kavian, R.; Graham, D. J.; Kim, D. Y.; Noda, S.; Nocera, D. G.; Shao-Horn, Y.; Lee, S. W. Electrochemical Polymerization of Pyrene Derivatives on Functionalized Carbon Nanotubes for Pseudocapacitive Electrodes. *Nat. Commun.* **2015**, *6*, 7040.

(36) Sato, S.; Unemoto, A.; Ikeda, T.; Orimo, S.-i.; Isobe, H. Carbon-Rich Active Materials with Macrocyclic Nanochannels for High-Capacity Negative Electrodes in All-Solid-State Lithium Rechargeable Batteries. *Small* **2016**, *12*, 3381−3387.

(37) Rodríguez-Pérez, I. A.; Bommier, C.; Fuller, D. D.; Leonard, D. P.; Williams, A. G.; Ji, X. Toward Higher Capacities of Hydrocarbon Cathodes in Dual-Ion Batteries. *ACS Appl. Mater. Interfaces* **2018**, *10*, 43311−43315.

(38) He, D.; Xiao, F.; Wang, Z.; He, A.; Liu, R.; Jin, G. Dynamic Hierarchical Self-Assemble Small Molecule Structure Hexabenzocoronene for the High-Performance Anodes Lithium Ion Storage. *Nanoscale Res. Lett.* **2019**, *14*, 65.

(39) Mitsuhashi, R.; Suzuki, Y.; Yamanari, Y.; Mitamura, H.; Kambe, T.; Ikeda, N.; Okamoto, H.; Fujiwara, A.; Yamaji, M.; Kawasaki, N.; Maniwa, Y.; Kubozono, Y. Superconductivity in Alkali-metal-doped Picene. *Nature* **2010**, *464*, 76−79.

(40) Takabayashi, Y.; Menelaou, M.; Tamura, H.; Takemori, N.; Koretsune, T.; Štefančič, A.; Klupp, G.; Buurma, A. J. C.; Nomura, Y.; Arita, R.; Arčon, D.; Rosseinsky, M. J.; Prassides, K. π-Electron S = 1/2 Quantum Spin-Liquid State in an Ionic Polyaromatic Hydrocarbon. *Nat. Chem.* **2017**, *9*, 635−643.

(41) Speight, J. G.; Kovacic, P.; Koch, F. W. Synthesis and Properties of Polyphenyls and Polyphenylenes. *J. Macromol. Sci. Rev. Macromol. Chem.* **1971**, *5*, 295−386.

(42) Kovacic, P.; Jones, M. B. Dehydro Coupling of Aromatic Nuclei by Catalyst-Oxidant Systems: Poly(p-phenylene). *Chem. Rev.* **1987**, *87*, 357−379.

(43) Clancy, A. J.; Bayazit, M. K.; Hodge, S. A.; Skipper, N. T.; Howard, C. A.; Shaffer, M. S. P. Charged Carbon Nanomaterials: Redox Chemistries of Fullerenes, Carbon Nanotubes, and Graphenes. *Chem. Rev.* **2018**, *118*, 7363−7408.

(44) Zhang, S. S. A Review on Electrolyte Additives for Lithium-Ion Batteries. *J. Power Sources* **2006**, *162*, 1379−1394.

(45) Abdulkarim, A.; Nathusius, M.; Bäuerle, R.; Strunk, K.-P.; Beck, S.; Räder, H. J.; Pucci, A.; Melzer, C.; Jänsch, D.; Freudenberg, J. Beyond *p*-Hexaphenylenes: Synthesis of Unsubstituted *p*-Nonaphenylene by a Precursor Protocol. *Chem. - Eur. J.* **2021**, *27*, 281−288.

(46) Baker, K. N.; Fratini, A. V.; Resch, T.; Knachel, H. C.; Adams, W. W.; Socci, E. P.; Farmer, B. L. Crystal Structures, Phase Transitions and Energy Calculations of Poly(*p*-phenylene) Oligomers. *Polymer* **1993**, *34*, 1571−1587.

(47) Darzi, E. R.; Jasti, R. The Dynamic, Size-Dependent Properties of [5]−[12]Cycloparaphenylenes. *Chem. Soc. Rev.* **2015**, *44*, 6401−6410.

(48) Iwamoto, T.; Watanabe, Y.; Sakamoto, Y.; Suzuki, T.; Yamago, S. Selective and Random Syntheses of [*n*]Cycloparaphenylenes (*n* = 8−13) and Size Dependence of their Electronic Properties. *J. Am. Chem. Soc.* **2011**, *133*, 8354−8361.

(49) Ivory, D. M.; Miller, G. G.; Sowa, J. M.; Shacklette, L. W.; Chance, R. R.; Baughman, R. H. Highly Conducting Charge-Transfer Complexes of Poly(*p*-phenylene). *J. Chem. Phys.* **1979**, *71*, 1506−1507.

(50) Guan, Y.-S.; Hu, Y.; Huang, Y.; Cannella, A. F.; Li, C.; Armstrong, J. N.; Ren, S. Alkali-Metal-Intercalated Aromatic Hydrocarbon Conductors. *ACS Appl. Nano Mater.* **2019**, *2*, 1140−1145.

(51) Hu, Y.; Zhong, G.; Guan, Y.-S.; Lee, N. H.; Zhang, Y.; Li, Y.; Mitchell, T.; Armstrong, J. N.; Benedict, J.; Hla, S.-W.; Ren, S. Alkali-Metal-Intercalated Percolation Network Regulates Self-Assembled Electronic Aromatic Molecules. *Adv. Mater.* **2019**, *31*, 1807178.

(52) Zhong, G.-H.; Yang, D.-Y.; Zhang, K.; Wang, R.-S.; Zhang, C.; Lin, H.-Q.; Chen, X.-J. Superconductivity and Phase Stability of Potassium-Doped Biphenyl. *Phys. Chem. Chem. Phys.* **2018**, *20*, 25217−25223.

(53) Huang, G.; Zhong, G.-H.; Wang, R.-S.; Han, J.-X.; Lin, H.-Q.; Chen, X.-J. Superconductivity and Phase Stability of Potassium-doped *p*-Quinquephenyl. *Carbon* **2019**, *143*, 837−843.

(54) Yan, J.-F.; Zhong, G.-H.; Wang, R.-S.; Zhang, K.; Lin, H.-Q.; Chen, X.-J. Superconductivity and Phase Stability of Potassium-Intercalated *p*-Quaterphenyl. *J. Phys. Chem. Lett.* **2019**, *10*, 40−47.

(55) Wang, R.-S.; Gao, Y.; Huang, Z.-B.; Chen, X.-J. Superconductivity above 120 K in a Chain Link Molecule. *arXiv (Superconductivity)*, 20 Mar 2017, 1703.06641, ver. 1. https://doi.org/10.48550/arXiv.1703.06641.

(56) Meerholz, K.; Heinze, J. Multiple Reversible Electrochemical Reduction of Aromatic Hydrocarbons in Liquid Alkylamines. *J. Am. Chem. Soc.* **1989**, *111*, 2325−2326.

(57) Paris, M.; Péres, L. O.; Chauvet, O.; Froyer, G. Solid-State NMR Study of Na versus K Doping of *para*-Phenylene Oligomers. *J. Phys. Chem. B* **2006**, *110*, 743−747.

(58) Sakamoto, A.; Harada, T.; Tonegawa, N. A New Approach to the Spectral Study of Unstable Radicals and Ions in Solution by the Use of an Inert Gas Glovebox System: Observation and Analysis of the Infrared Spectra of the Radical Anion and Dianion of *p*-Terphenyl. *J. Phys. Chem. B* **2008**, *112*, 1180−1187.

(59) Péres, L. O.; Spiesser, M.; Froyer, G. Reduction of *p*-Terphenyl, *p*-Quaterphenyl and *p*-Sexiphenyl using Alkali Metal in Liquid Ammonia: Process and Characterization of the Reduced Compounds. *Synth. Met.* **2005**, *155*, 450−454.

(60) Furuya, K.; Torii, H.; Furukawa, Y.; Tasumi, M. Density Functional Study on the Structures and Vibrational Spectra of the Radical Anion and Cation of Biphenyl. *J. Mol. Struct.: THEOCHEM* **1998**, *424*, 225−235.

(61) de la Viuda, M.; Yus, M.; Guijarro, A. On the Nature of Lithium Biphenyl in Ethereal Solvents. A Critical Analysis Unifying DFT Calculations, Physicochemical Data in Solution, and a X-ray Structure. *J. Phys. Chem. B* **2011**, *115*, 14610−14616.

(62) Schlenk, W.; Bergmann, E. Forschungen auf dem Gebiete der Alkaliorganischen Verbindungen. I. Über Produkte der Addition von Alkalimetal an Mehrfache Kohlenstoff-Kohlenstoff-Bindungen. *Liebigs Ann. Chem.* **1928**, *463*, 1−97.

(63) Noordik, J. H.; Schreurs, J.; Gould, R. O.; Mooij, J. J.; De Boer, E. Molecular and Magnetic Structure of the Paramagnetic Ion Pair Bis(tetraglyme)potassium Biphenyl. *J. Phys. Chem.* **1978**, *82*, 1105−1110.

(64) Noordik, J. H.; Doesburg, H. M.; Prick, P. A. J. Structures of the Sodium−*p*-terphenyl Ion Pairs: Disodium Derphenylide−tetrahydrofuran (1/6) and Disodium Diterphenylide Terphenyl−1,2-dimethoxyethane (1/6). *Acta Crystallogr., Sect. B: Struct. Crystallogr. Cryst. Chem.* **1981**, *37*, 1659−1663.

(65) Bock, H.; Gharagozloo-Hubmann, K.; Sievert, M. Interaction in Molecular Crystals, 160 [1, 2]. Crystallization and Structure Determination of the Different Polyphenyl Contact Ion Multiples $[p\text{-quaterphenyl}^{\ominus\ominus}][Na^{\oplus}(DME)_3]_2$, $[p\text{-quaterphenyl}^{\ominus\ominus}(Na^{\oplus}(THF)_3)_2]$ and $[p\text{-terphenyl}^{\ominus\ominus}Na^{\oplus}(DME)_2Na^{\oplus}(DME)]_2$. *Z. Naturforsch., B: J. Chem. Sci.* **2000**, *55*, 1103−1113.

(66) Furukawa, Y.; Ohtsuka, H.; Tasumi, M. Raman Studies of Polarons and Bipolarons in Sodium-Doped Poly-*p*-phenylene. *Synth. Met.* **1993**, *55*, 516−523.

(67) Zhou, Z.; Zhu, Y.; Wei, Z.; Bergner, J.; Neiß, C.; Doloczki, S.; Görling, A.; Kivala, M.; Petrukhina, M. A. Reduction of *π*-Expanded Cyclooctatetraene with Lithium: Stabilization of the Tetraanion through Internal Li$^+$ Coordination. *Angew. Chem. Int. Ed* **2021**, *60*, 3510−3514.

(68) Pennachio, M.; Zhou, Z.; Wei, Z.; Liu, S.; Rogachev, A. Yu.; Petrukhina, M. A. Doubly-Reduced Pentacene in Different Coordination Environments: X-ray Crystallographic and Theoretical Insights into Structural and Electronic Changes. *Chem. - Eur. J.* **2022**, *28*, No. e202104194.

(69) Zabula, A. V.; Spisak, S. N.; Filatov, A. S.; Grigoryants, V. M.; Petrukhina, M. A. How Charging Corannulene with One and Two Electrons Affects Its Geometry and Aggregation with Sodium and Potassium Cations. *Chem. - Eur. J.* **2012**, *18*, 6476−6484.

(70) Zhu, Y.; Zhou, Z.; Wei, Z.; Petrukhina, M. A. Two-Fold Reduction of Dibenzo[*a,e*]cyclooctatetraene with Group 1 Metals: From Lithium to Cesium. *Organometallics* **2020**, *39*, 4688−4695.

(71) Zhou, Z.; Zhu, Y.; Fernández-García, J. M.; Wei, Z.; Fernández, I.; Petrukhina, M. A.; Martín, N. Stepwise Reduction of a Corannulene-Based Helical Molecular Nanographene with Na Metal. *Chem. Commun.* **2022**, *58*, 5574−5577.

(72) Spisak, S. N.; Wei, Z.; Darzi, E.; Jasti, R.; Petrukhina, M. A. Highly Strained [6]Cycloparaphenylene: Crystallization of an Unsolvated Polymorph and the First Mono- and Dianions. *Chem. Commun.* **2018**, *54*, 7818−7821.

(73) Zhou, Z.; Wei, Z.; Schaub, T. A.; Jasti, R.; Petrukhina, M. A. Structural Deformation and Host−Guest Properties of Doubly-Reduced Cycloparaphenylenes, [*n*]CPPs$^{2−}$ (*n* = 6, 8, 10, and 12). *Chem. Sci.* **2020**, *11*, 9395−9401.

(74) Zhou, Z.; Wei, Z.; Ikemoto, K.; Sato, S.; Isobe, H.; Petrukhina, M. A. Chemical Reduction of Nanosized [6]Cyclo-2,7-naphthylene Macrocycle. *Angew. Chem. Int. Ed* **2021**, *60*, 11201−11205.

(75) Spisak, S. N.; Zabula, A. V.; Filatov, A. S.; Rogachev, A. Yu.; Petrukhina, M. A. Selective *Endo* and *Exo* Binding of Alkali Metals to Corannulene. *Angew. Chem. Int. Ed* **2011**, *50*, 8090−8094.

(76) Zhou, Z.; Fernández-García, J. M.; Zhu, Y.; Evans, P. J.; Rodríguez, R.; Crassous, J.; Wei, Z.; Fernández, I.; Petrukhina, M. A.; Martín, N. Site-Specific Reduction-Induced Hydrogenation of a Helical Bilayer Nanographene with K and Rb Metals: Electron Multiaddition and Selective Rb$^+$ Complexation. *Angew. Chem., Int. Ed* **2022**, *61*, No. e202115747.

(77) Zhou, Z.; Üngör, Ö.; Wei, Z.; Shatruk, M.; Tsybizova, A.; Gershoni-Poranne, R.; Petrukhina, M. A. Tuning Magnetic Inter-

actions Between Triphenylene Radicals by Variation of Crystal Packing in Structures with Alkali Metal Counterions. *Inorg. Chem.* **2021**, *60*, 14844−14853.

(78) Gershoni-Poranne, R.; Rahalkar, A. P.; Stanger, A. The Predictive Power of Aromaticity: Quantitative Correlation between Aromaticity and Ionization Potentials and HOMO−LUMO Gaps in Oligomers of Benzene, Pyrrole, Furan, and Thiophene. *Phys. Chem. Chem. Phys.* **2018**, *20*, 14808−14817.

(79) Kozhemyakina, N. V.; Nuss, J.; Jansen, M. Demonstration of the "Break-and-Seal" Approach to Fullerides of Complex Cations at the Example of $KC_{60}(THF)_5$·2THF. *Z. Anorg. Allg. Chem.* **2009**, *635*, 1355−1361.

(80) *SAINT, part of Bruker APEX3 software package*, version 2017.3−0; Bruker AXS, Inc.: Madison, WI, 2017.

(81) Sheldrick, G. M. *SADABS, part of Bruker APEX3 software package*, version 2017.3−0; Bruker AXS, Inc.: Madison, WI, 2017.

(82) Sheldrick, G. M. SHELXT - Integrated Space-Group and Crystal-Structure Determination. *Acta Crystallogr., Sect. A: Found. Adv.* **2015**, *71*, 3−8.

(83) Sheldrick, G. M. Crystal Structure Refinement with SHELXL. *Acta Crystallogr.* **2015**, *C71*, 3−8.

(84) Dolomanov, O. V.; Bourhis, L. J.; Gildea, R. J.; Howard, J. A. K.; Puschmann, H. OLEX2: A Complete Structure Solution, Refinement and Analysis Program. *J. Appl. Crystallogr.* **2009**, *42*, 339−341.

(85) Neese, F.; Wennmohs, F.; Becker, U.; Riplinger, C. The ORCA Quantum Chemistry Program Package. *J. Chem. Phys.* **2020**, *152*, 224108.

(86) Perdew, J. P.; Burke, K.; Ernzerhof, M. Generalized Gradient Approximation Made Simple. *Phys. Rev. Lett.* **1996**, *77*, 3865−3868.

(87) Adamo, C.; Barone, V. Toward Reliable Density Functional Methods Without Adjustable Parameters: The PBE0Model. *J. Chem. Phys.* **1999**, *110*, 6158−6170.

(88) Weigend, F.; Ahlrichs, R. Balanced Basis Sets of Split Valence, Triple Zeta Valence and Quadruple Zeta Valence Quality for H to Rn: Design and Assessment of Accuracy. *Phys. Chem. Chem. Phys.* **2005**, *7*, 3297−3305.

(89) Rappoport, D.; Furche, F. Property-optimized Gaussian Basis Sets for Molecular Response Calculations. *J. Chem. Phys.* **2010**, *133*, 134105.

(90) Grimme, S.; Antony, J.; Ehrlich, S.; Krieg, H. A. Consistent and Accurate *ab* Initio Parametrization of Density Functional Dispersion Correction (DFT-D) for the 94 Elements H-Pu. *J. Chem. Phys.* **2010**, *132*, 154104.

(91) Grimme, S.; Ehrlich, S.; Goerigk, L. Effect of the Damping Function in Dispersion Corrected Density Functional Theory. *J. Comput. Chem.* **2011**, *32*, 1456−1465.

(92) Schleyer, P. v. R.; Maerker, C.; Dransfeld, A.; Jiao, H.; van Eikema Hommes, N. J. R. Nucleus-Independent Chemical Shifts: A Simple and Efficient Aromaticity Probe. *J. Am. Chem. Soc.* **1996**, *118*, 6317−6318.

(93) Gershoni-Poranne, R.; Stanger, A. NICS − Nucleus Independent Chemical Shift. In *Aromaticity: Modern Computational Methods and Applications*; Fernandez, I., Ed.; Elsevier, 2021; pp 99−154.

(94) Rahalkar, A. P.; Stanger, A. *Aroma*, 2014. https://chemistry.technion.ac.il/en/team/amnon-stanger/.

(95) Geuenich, D.; Herges, R. *J. Phys. Chem. A* **2001**, *105*, 3214−3220.

(96) Geuenich, D.; Hess, K.; Koehler, F.; Herges, R. *Chem. Rev.* **2005**, *105*, 3758−3772.

(97) Frisch, M. J.; Trucks, G. W.; Schlegel, H. B.; Scuseria, G. E.; Robb, M. A.; Cheeseman, J. R.; Scalmani, G.; Barone, V.; Mennucci, B.; Petersson, G. A.; Nakatsuji, H.; Caricato, M.; Li, X.; Hratchian, H. P.; Izmaylov, A. F.; Bloino, J.; Zheng, G.; Sonnenberg, J. L.; Hada, M.; Ehara, M.; Toyota, K.; Fukuda, R.; Hasegawa, J.; Ishida, M.; Nakajima, T.; Honda, Y.; Kitao, O.; Nakai, H.; Vreven, T.; Montgomery, J. A., Jr.; Peralta, J. E.; Ogliaro, F.; Bearpark, M.; Heyd, J. J.; Brothers, E.; Kudin, K. N.; Staroverov, V. N.; Kobayashi, R.; Normand, J.; Raghavachari, K.; Rendell, A.; Burant, J. C.; Iyengar, S. S.; Tomasi, J.; Cossi, M.; Rega, N.; Millam, J. M.; Klene, M.; Knox, J. E.; Cross, J. B.; Bakken, V.; Adamo, C.; Jaramillo, J.; Gomperts, R.; Stratmann, R. E.; Yazyev, O.; Austin, A. J.; Cammi, R.; Pomelli, C.; Ochterski, J. W.; Martin, R. L.; Morokuma, K.; Zakrzewski, V. G.; Voth, G. A.; Salvador, P.; Dannenberg, J. J.; Dapprich, S.; Daniels, A. D.; Farkas, O.; Foresman, J. B.; Ortiz, J. V.; Cioslowski, J.; Fox, D. J. *Gaussian 09*, revision D.01; Gaussian, Inc.: Wallingford, CT, 2009.